

X-ray/Optical Bursts from GS 1826–24

A.K.H. Kong¹, L. Homer¹, E. Kuulkers^{2,3}, P.A. Charles¹ and A.P. Smale⁴

¹ Department of Astrophysics, Nuclear & Astrophysics Laboratory, Keble Road, Oxford OX1 3RH

² Space Research Organization Netherlands, Sorbonnelaan 2, 3584 CA Utrecht, The Netherlands

³ Astronomical Institute, Utrecht University, P.O. Box 80000, 3507 TA Utrecht, The Netherlands

⁴ Laboratory for High Energy Astrophysics, Code 660.2, NASA Goddard Space Flight Center, Greenbelt, MD 20771, USA

Accepted. Received.

ABSTRACT

We report results from the first simultaneous X-ray (*RXTE*) and optical (SAAO) observations of the low-mass X-ray binary GS 1826–24 in June 1998. A type-I burst was detected in both X-ray and optical wavelengths. Its energy-dependent profile, energetics and spectral evolution provide evidence for an increase in the X-ray burning area but not for photospheric radius expansion. However, we may still derive an upper limit for its distance of 7.5 ± 0.5 kpc, assuming a peak flux of $\sim 2.8 \times 10^{-8}$ erg cm $^{-2}$ s $^{-1}$. A ~ 3 s optical delay with respect to the X-ray burst is also observed and we infer that this is related to the X-ray reprocessing in the accretion disk into the optical. This provides support for the recently proposed orbital period of ~ 2 h. We also present an *ASCA* observation from March 1998, during which two X-ray bursts were detected.

Key words: accretion, accretion disks – binaries: close – stars: individual (GS 1826–24) – X-rays: bursts

1 INTRODUCTION

GS 1826–24 was discovered serendipitously in 1988 by the *Ginga* satellite (Makino et al. 1988) at an average flux of 26 mCrab (1–40 keV) and was fitted by a single power law spectrum with $\alpha \sim 1.7$. Whilst showing some evidence for variability during 1988–89 (Tanaka & Lewin 1995; In’t Zand 1992), *ROSAT* PSPC observations in 1990 and 1992 (Barret et al. 1995) found comparable flux levels and no X-ray bursts were detected during 8 hours exposure on the source. The spectrum was well fitted by a single power law with $\alpha \sim 1.5 – 1.8$ and an absorption column, $N_H \sim 5 \times 10^{21}$ cm $^{-2}$. Temporal analysis of both the *Ginga* and *ROSAT* data yielded a featureless f^{-1} power spectrum extending from 10 $^{-4}$ –500 Hz (Tanaka & Lewin 1995; Barret et al. 1995), with neither quasi-periodic oscillations (QPOs) nor pulsations being detected.

Since there was no detection prior to *Ginga*, the source was catalogued as an X-ray transient. Its similarities to Cyg X-1 and GX 339–4 in the low state, both in spectrum and temporal behaviour (hard X-ray spectrum and strong flickering), led to an early suggestion by Tanaka (1989) that it was a soft X-ray transient with a possible black-hole primary. Following its detection by *CGRO* OSSE in the 60–200 keV energy range, Strickman et al. (1996) doubted the suggestion of a black-hole primary after examining the combined spectrum from both *Ginga* and OSSE. They found that this

required a model with an exponentially cut-off power law plus reflection term. The observed cut-off energy around 58 keV is typical of the cooler neutron star hard X-ray spectra. The suggestion that GS 1826–24 contains a neutron star was also discussed in detail by Barret et al. (1996), where they compared the luminosity of the source with other X-ray bursters. The recent report of 70 X-ray bursts in 2.5 years by *BeppoSAX* WFC (Ubertini et al. 1999) and an optical burst by Homer et al. (1998) confirms the presence of a neutron star accretor.

Following the first *ROSAT* PSPC all-sky survey observations in September 1990, and the determination of a preliminary X-ray position, a search for the counterpart yielded a time variable, UV-excess, emission line star (Motch et al. 1994; Barret et al. 1995). The source had $B = 19.7$, and an uncertain V magnitude (~ 19.3), due to contamination by a nearby star. Subsequent high-speed CCD photometry by Homer et al. (1998) yielded a ~ 2.1 hr optical modulation, but confirmation of its stability requires observation over a longer time interval. We therefore carried out an *ASCA* observation and simultaneous *RXTE*/optical observations of GS 1826–24 in order to study its spectral behaviour and very short timescale variability, as well as the 2.1 hr optical modulation. In Table 1, we summarize the *ASCA*, *RXTE* and SAAO observations used in this work.

This paper is structured as follows. An outline of all the X-ray and optical observations is given in section 2. In sec-

Table 1. A Journal of the X-ray/optical observations of GS 1826–24

Observatory	Detector	Date	Time (UT)	
			Start	End
<i>ASCA</i>	SIS+GIS	31.03.98	10:52	20:54
		23.06.98	19:20	21:59
		24.06.98	19:20	21:58
		25.06.98	19:21	21:57
		28.07.98	08:12	14:22
		29.07.98	13:05	15:51
SAAO	1.9m+UCT CCD	23.06.98	19:08	04:57
		24.06.98	19:07	03:17
		25.06.98	18:36	04:11

tion 3 we report the spectral analysis of *ASCA* data for both persistent and burst emission. Simultaneous *RXTE*/optical observations, including the analysis of a simultaneous X-ray/optical burst are also presented. We discuss the implications of the X-ray bursts and constrain the nature of the source from the delay between the X-rays and optical in section 4. We present the overall timing study of the *ASCA* and *RXTE*/optical observations in a companion paper (Homer et al. 1999, henceforth paper II).

2 OBSERVATIONS AND DATA REDUCTION

2.1 *ASCA*

The *ASCA* satellite consists of four co-aligned telescopes, each of which is a conical foil mirror that focuses X-rays onto two Solid State Imaging Spectrometers (SIS) and two Gas Imaging Spectrometers (GIS) (Tanaka, Inoue & Holt 1994). The SIS detectors are sensitive to photons in the 0.4–10.0 keV energy band with nominal spectral resolution of 2% at 6 keV. The GIS detectors provide imaging in the 0.7–10 keV energy range and have a relatively modest spectral resolution of 8% at 6 keV, in comparison to the SIS, but with a larger effective area at higher energies.

For our observation of GS 1826–24 on 1998 March 31 (see Table 1), one CCD was activated for each SIS, giving an $11' \times 11'$ field of field and temporal resolution of 4 s. The GIS detectors were set to MPC mode (i.e. no image could be extracted) so that the temporal resolution would be improved to 0.5 s.

The data were filtered with standard criteria including the rejection of hot and flickering pixels and event grade selection. We extracted the SIS source spectra from circular regions of $3'$ radius, yielding 11.2 ks total exposure. The background spectra were extracted from source-free regions of the instruments during the same observation. For GIS, after the standard selection procedure, the net on-source time was 18.9 ks.

2.2 *RXTE*

We also observed GS 1826–24 with the Proportional Counter Array (PCA) instrument on *RXTE* (Bradt, Rothschild & Swank 1993) between 1998 June 23 and July 29 (see Table 1). The PCA consists of five nearly identical Proportional Counter Units (PCUs) sensitive to X-rays with en-

ergy range between 2–60 keV and a total effective area of $\sim 6500 \text{ cm}^2$. The PCUs each have a multi-anode xenon-filled volume, with a front propane volume which is primarily used for background rejection. For the entire PCA and across the complete energy band, the Crab Nebula produces a count rate of 13,000 counts s^{-1} . The PCA spectral resolution at 6 keV is approximately 18% and the maximum timing resolution available was 1 μs . However, in order to maximize our timing and spectral resolution, we adopted a $125\mu\text{s}$ time resolution, 64 spectral energy channel mode over 2–60 keV in addition to the standard mode configuration. All light curves and spectra presented here have been corrected for background and dead-time. For most of the time, at least four PCUs were turned on, and so we utilized only data from these PCUs in order to minimize systematic uncertainties.

2.3 Optical

Observations of a small (50×33 arcsecs) region surrounding the optical counterpart of GS 1826–24 were made using the UCT-CCD fast photometer (O'Donoghue 1995), at the Cassegrain focus of the 1.9m telescope at SAAO, Sutherland from 1998 June 23 to 26. The UCT-CCD fast photometer is a Wright Camera 576×420 coated GEC CCD which was used here half-masked so as to operate in frame transfer mode, allowing exposures of as short as 2 s with no dead-time. The conditions were generally good with typical seeing $\sim 1.5\text{--}2.5$ arcsec and the timing resolution for the source was 5 s. An observing log is presented in Table 1. We performed data reduction using IRAF, including photometry with the implementation of DAOPHOT II (Stetson 1987). Due to moderate crowding of the counterpart with a nearby but fainter neighbour and the variable seeing, point spread function (PSF) fitting was employed in order to obtain good photometry. The details of this procedure are given in Homer et al. (1998).

3 ANALYSIS AND RESULTS

3.1 *ASCA* Observations

Given the better spectral resolution and higher sensitivity below 2 keV of the SIS detectors, we use those data to study the persistent emission of GS 1826–24. The spectrum (excluding the burst intervals, see below) was fitted with a blackbody plus a power law component. The fit quality was good, with $\chi^2_\nu = 1.14$ for 307 degrees of freedom (d.o.f.) and these results are summarized in Table 2 and Fig. 1 (whenever an error for a spectral parameter is quoted throughout this paper, it refers to the single parameter 1σ error).

Our results are consistent with those obtained by In't Zand et al. (1999) using the *BeppoSAX* NFI, taken six days later. Moreover, their 2–10 keV flux of $5.41 \times 10^{-10} \text{ erg cm}^{-2} \text{ s}^{-1}$ which is only $\sim 9\%$ smaller than our determination, is consistent with the $\sim 10\%$ fall in count rate seen by the *RXTE* ASM during that interval.

Two X-ray bursts were detected by the *ASCA* GIS and one of them was caught by SIS. The time interval between the two bursts was ~ 5.4 hr and is consistent with the 5.76 ± 0.6 hr quasi-periodicity of the burst recurrence as found by *BeppoSAX* WFC observations (Ubertini et al. 1999). Figure

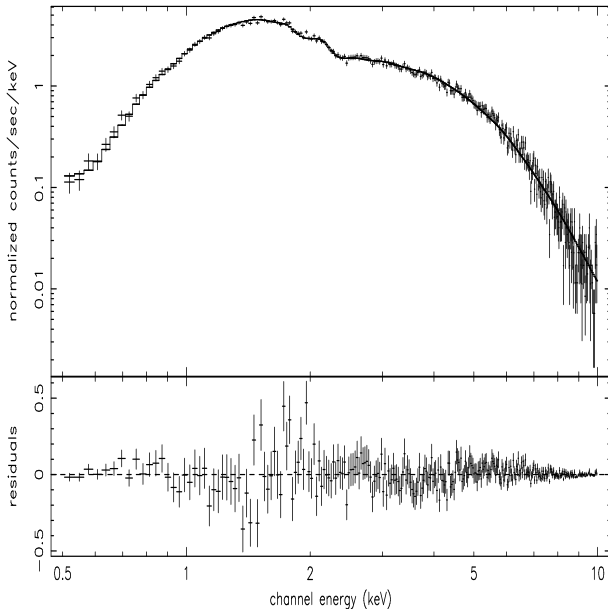


Figure 1. Upper panel: *ASCA* SIS spectral fit to GS 1826-24 persistent emission. The spectrum was fitted with a blackbody ($kT = 0.74 \pm 0.02$ keV) plus a power law component ($\alpha = 1.11 \pm 0.09$). Lower panel: residuals in units of σ .

Table 2. GS 1826-24 persistent emission SIS spectral fit. The errors are single parameter 1σ errors.

Model	Power law plus blackbody
N_H	$(4.0 \pm 0.36) \times 10^{21}$ cm $^{-2}$
kT_{bb}^a	0.74 ± 0.02 keV
R_{bb} at 8 kpc b	11.3 ± 0.6 km
Photon index, α	1.11 ± 0.09
χ^2 (307 d.o.f.)	1.14
Flux 0.5–10 keV	$(6.8 \pm 0.2) \times 10^{-10}$ erg cm $^{-2}$ s $^{-1}$
Flux 2–10 keV	$(5.9 \pm 0.2) \times 10^{-10}$ erg cm $^{-2}$ s $^{-1}$

a Blackbody temperature

b Blackbody radius

2 shows the time profiles of the two bursts in the 0.7–10 keV range with 4 s binning. Their rise times (difference between time of the peak and time of the start of the burst using a linear-rise exponential-decay model) and e-folding times are comparable, see Table 3.

Since the GIS was set to MPC mode, which has no positional information, the lack of background estimation limits the usefulness of the spectra. We therefore here analyse the first burst which was detected with SIS.

Table 3. Timing parameters of the two bursts by fitting linear-rise exponential-decay model.

	burst 1	burst 2
Peak time (MJD)	50903.628	50903.853
Rise time (s)	6.7 ± 0.2	8.8 ± 0.02
e-folding time (s)	55 ± 1.8	50.8 ± 1.9
Peak flux (0.7–10 keV; Crab units)	0.22	0.23

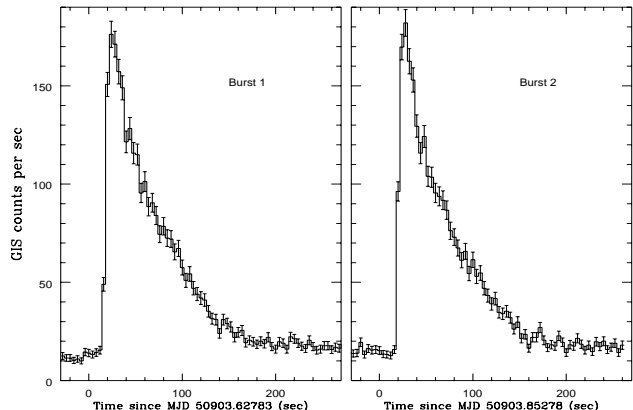


Figure 2. The time profiles of the two X-ray bursts in the 0.7–10 keV range at a time resolution of 4 s as observed by the *ASCA* GIS in March, 1998.

We extracted a series of spectral slices through the burst with 4 s time resolution in the rising phase and 20 s resolution during decay. Spectral analyses of these slices were performed over the 0.5–10 keV range using a variety of approaches. The most straightforward ‘standard’ approach was to choose a 300 s section of data immediately prior to the burst and use this as our ‘background’ for spectral fits to the individual spectra through the burst. The net (burst – ‘background’) emission was well fitted ($\chi^2_\nu \sim 0.6 – 1.2$) with a simple blackbody. Figure 3 (left) shows the time variation of the bolometric flux, blackbody temperature and radius assuming a distance of 8 kpc (In’t Zand et al. 1999). The radii are rather low (~ 4 km) and show an anti-correlation with temperature.

However, the analysis of X-ray burst data can be complicated in cases where the persistent emission contains a blackbody contribution from the outer layers of the neutron star. Failing to account for this component may lead to errors in the temperature determination and severe underestimates in the derived blackbody radius during the later stages of the burst (van Paradijs & Lewin 1985). We thus repeated our analysis, fitting the above two-component model to each gross (continuum + burst) spectrum, rather than a single blackbody component to the net burst spectrum. The power-law component was held constant at its continuum emission value while the blackbody component was permitted to vary. The results of our two-component spectral fits are shown in Figure 3 (right), once again for an assumed distance of 8 kpc. The most important difference with the results of the ‘standard’ approach is that the blackbody radius is now in the range for a typical neutron star (~ 10 km). The blackbody radii show moderate variations, which appear to be anti-correlated with temperature. This indicates that the blackbody radiation from the neutron star contributes significantly to the persistent emission. The blackbody temperatures are higher during the beginning of the burst and then decline as expected for a type I burst (see Figure 3).

The change of the apparent blackbody radius may be affected by the non-Planckian shape of the spectrum of a hot neutron star (see Sztajno et al. 1986 and references therein). As a result, the temperature fitted using a blackbody is sim-

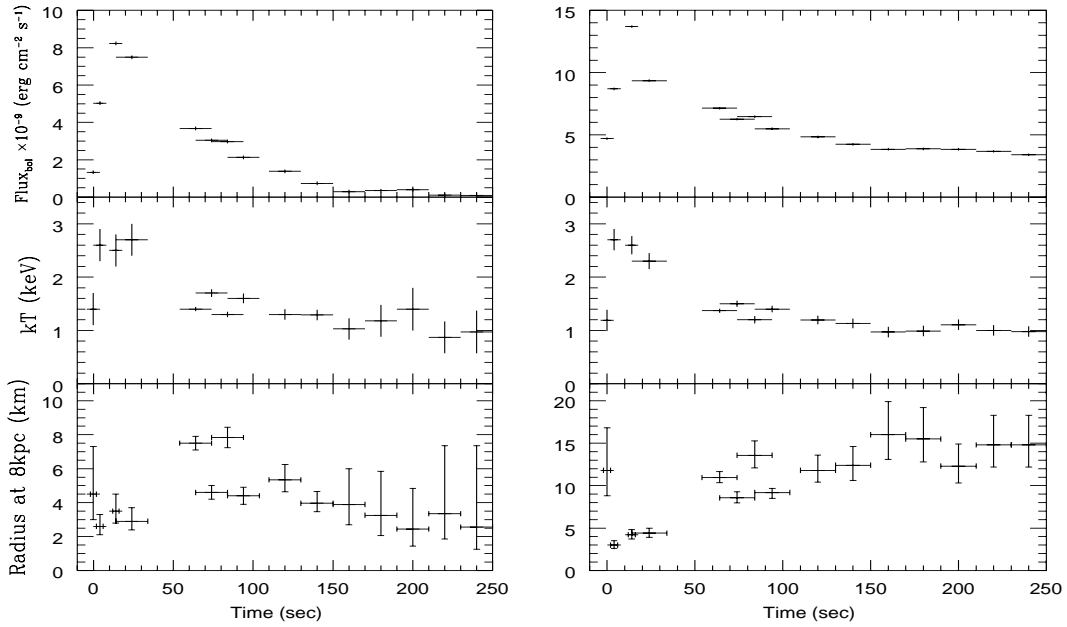


Figure 3. Results of the spectral analysis of net burst (left) and gross burst (right) emission from *ASCA*. Plotted are the variation of the flux (top), blackbody temperature (middle) and blackbody radius (bottom).

ply a ‘colour temperature’ (T_{bb}) which is higher than the effective temperature (T_{eff}); the ratio of T_{bb}/T_{eff} increases with T_{eff} (e.g. London, Taam & Howard 1984). Moreover the fitted blackbody radii are also affected, and so we used the average relation between blackbody radius and temperature obtained for 4U 1636–53 (Sztajno et al. 1985) to make an empirical correction to the radii obtained from the above two-component fits (see van Paradijs et al. 1986). As this method is strictly empirical, it is independent of possible uncertainties in model-atmosphere calculations (e.g. Sztajno et al. 1986). We have assumed that the radii are unaffected for $kT_{bb} < 1.25$ keV whilst for $kT_{bb} > 1.25$ keV the radii decrease linearly with temperature (e.g. van Paradijs et al. 1986).

The blackbody radii obtained following this final stage of the analysis (see Figure 4) do not show significant differences compared with the gross spectral analysis except that the radii during the peak of the burst are now in the range for a typical neutron star. There is no evidence for photospheric expansion since the radius remains almost constant throughout the burst (Figure 4). We also plotted the flux F_{bol} versus $F_{bol}^{1/4}/kT_{bb}$ but we do not find evidence for any increase of the X-ray emitting area (Strohmayer, Zhang & Swank 1997). This ratio is a constant proportional to $(R/d)^{1/2}$, where R and d are the radius and distance of the source if we assume it is blackbody emission from a spherical surface. The unabsorbed bolometric peak flux of the blackbody radiation and other burst parameters are listed in Table 4. The ratio of the average luminosity emitted in the persistent emission (since the previous burst) and that emitted in the burst, $L_{pers}/L_{burst} = 55 \pm 5$ assuming the separation of the two bursts is 5.4 hr.

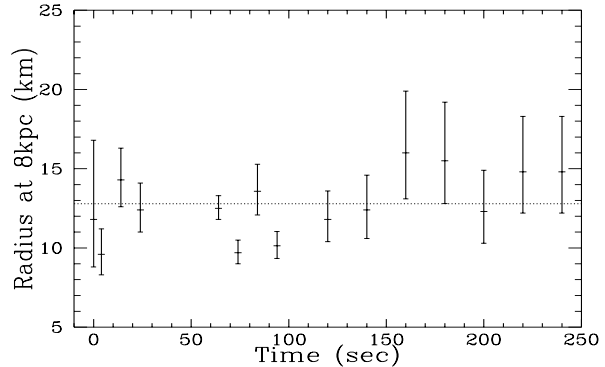


Figure 4. Variation of the blackbody radius of the gross burst emission (burst plus persistent) after correction for the deviation of the spectrum of a hot neutron star from a pure blackbody spectrum (see text for explanation). The dashed line is the mean blackbody radius.

3.2 Simultaneous *RXTE*/Optical Burst Analysis

During simultaneous X-ray/optical observations on 24 June 1998, both *RXTE* PCA and the SAAO 1.9m + UCT CCD detected a burst (see Figure 5). The burst lasted for ~ 150 s and the time profiles of the burst in both X-ray and optical are of the fast-rise exponential-decay form with the e-folding times in the different energy bands given in Table 5. The optical and X-ray bursts started almost at the same time but a delay is present between the peaks. The optical burst resembles the low energy (2–3.5 and 3.5–6.4 keV) X-ray light curves in which they all have a flat peak and a shoulder during the decay phase. At higher energies (> 6.4 keV), the peak is much sharper and the decay is faster during the initial decay phase.

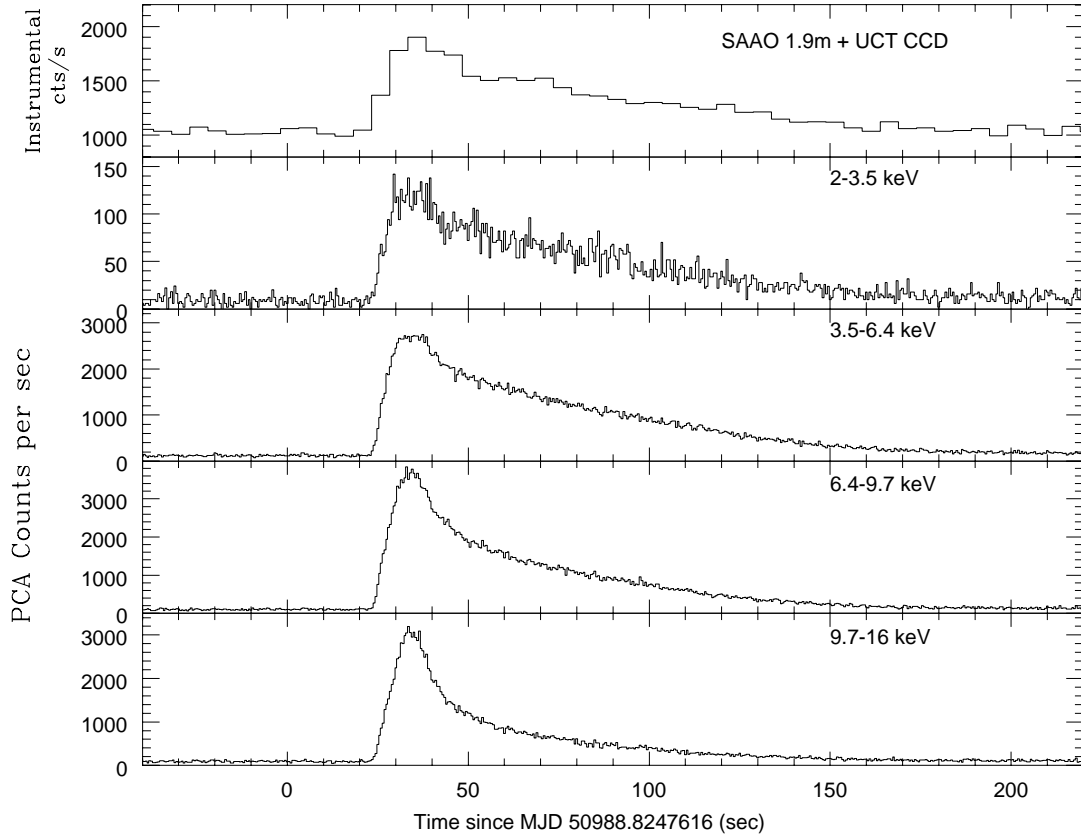


Figure 5. The optical (SAAO) and X-ray (*RXTE*) burst profiles in various energy bands. The timing resolution is 5 s (optical) and 0.5 s (*RXTE*/PCA). The decay times strongly depend on photon energy with decays being shorter at higher energies.

Table 4. Burst parameters for the *ASCA* and *RXTE* bursts

Burst	F_{max}^a (10^{-8} erg cm $^{-2}$ s $^{-1}$)	E_{burst}^b (10^{-5} erg cm $^{-2}$)	E_{pers}^c (10^{-5} erg cm $^{-2}$)	L_{pers}/L_{burst} (E_{pers}/E_{burst})	γ (F_{pers}/F_{max})	τ (E_{burst}/F_{max})
<i>ASCA</i>	3.0	0.13	7.1 ^d	54.6	0.12	43.3 s
<i>RXTE</i>	2.77	0.11	5.5 ^e	50	0.1	39.7 s

^a Unabsorbed bolometric peak flux

^b Total burst fluence

^c Persistent emission fluence

^d Assuming 5.4 hr burst separation

^e Assuming 5.76 hr burst separation

X-ray spectral analysis is performed in the same way as for the *ASCA* data. The persistent emission is fitted with a single power-law spectrum with $N_H = (7.3 \pm 1.5) \times 10^{21}$ cm $^{-2}$ and photon index, $\alpha = 1.7 \pm 0.01$ ($\chi^2_\nu = 1.11$ for 23 d.o.f.) which reveals an absorbed flux of $(1.2 \pm 0.01) \times 10^{-9}$ erg cm $^{-2}$ s $^{-1}$ in the 2–20 keV range. The photon index, α is much higher than that seen by *ASCA* and suggests a softer spectrum during the *RXTE* observations. We also perform spectral fitting with a power-law plus blackbody model but the fit does not improve and leads to a large error in N_H . Both the ‘standard’ method (net burst spectrum) and gross spectrum were almost indistinguishable from those presented in

Figure 6, presumably because the blackbody provides such a small contribution to the continuum emission. We also undertook the non-Planckian analysis as mentioned in the previous section, with results very similar to Figure 6, indicating that the effect due to the non-Planckian shape of the neutron star spectrum is very small. Once again the neutron star shows the spectral cooling during the burst typical of a type-I burst. The unabsorbed bolometric peak flux of the blackbody radiation and other burst parameters are listed in Table 4. The ratio $L_{pers}/L_{burst} = 50 \pm 4$ if we assume that the separation of two bursts is 5.76 hr (Ubertini et al. 1999).

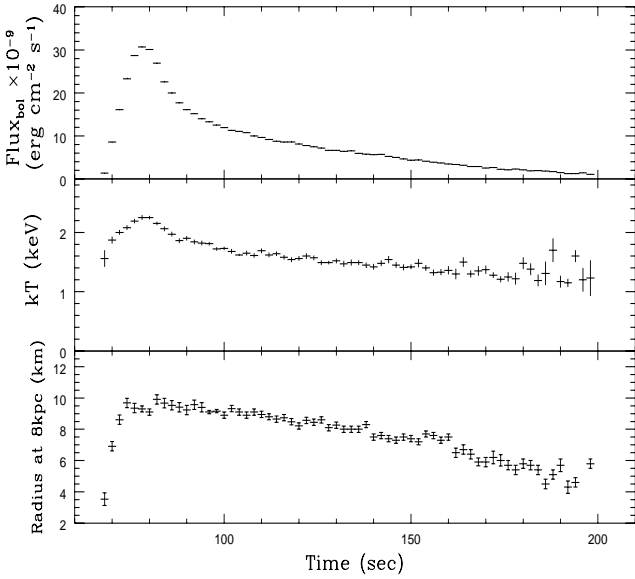


Figure 6. The variation of the flux, blackbody temperature and radius during the burst detected by *RXTE*. See text for explanation.

The blackbody radius increases to a maximum as the burst rises, but does not show the simultaneous drop in kT_{bb} and increase in R_{bb} that is the overt signature of photospheric radius expansion (see Lewin, van Paradijs & Taam 1995). However, when we plot the flux F_{bol} versus $F_{bol}^{1/4}/kT_{bb} \propto (R/d)^{1/2}$ we do find evidence for an increase in the X-ray burning area on the star (Strohmayer, Zhang & Swank 1997). This is shown in Figure 7 where the burst begins in the lower left and evolves diagonally to the upper right and then across to the left at an essentially constant value until near the end of the burst. This is an indication that indeed the X-ray burning area is not a constant but increases with time during the rising phase. $F_{bol}^{1/4}/kT_{bb}$ eventually reaches a nearly constant value and the neutron star surface simply cools during the decay phase.

Kilohertz QPOs between 200 and 1200 Hz were not detected during the burst with an upper limit of 1% (at 99% confidence). We also set upper limits on the presence of any coherent pulsations during the burst: < 1% between 100–500 Hz and 600–1200 Hz, and < 3% between 1000–4000 Hz (the Nyquist limit). A detailed timing analysis of the remaining simultaneous X-ray/optical data will be presented in paper II.

3.2.1 X-ray/optical time delay

Figure 5 shows the simultaneous optical/X-ray burst in different energy bands where there is a few seconds delay at the peak of the burst. In order to quantify this delay, we performed: (i) cross-correlation analysis, (ii) modelled the optical burst by convolving the X-ray light curve with a Gaussian transfer function.

3.2.1.1 Cross-correlation

We cross-correlated the optical data with X-ray data from different energy bands as well as the total (2–60 keV)

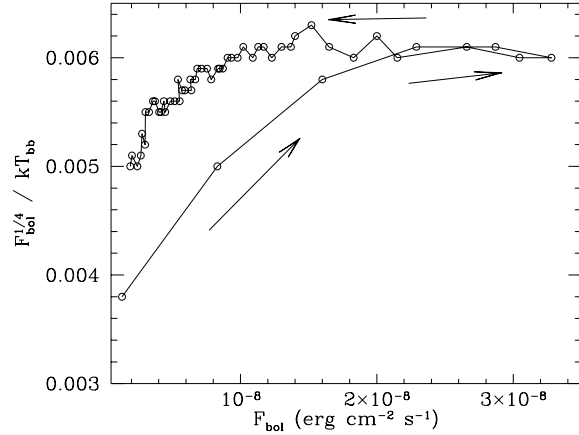


Figure 7. Plot of bolometric flux F_{bol} vs. $F_{bol}^{1/4}/kT_{bb}$ for the *RXTE* burst. The burst evolves from the lower left to upper right and then crosses to the left at nearly constant $F_{bol}^{1/4}/kT_{bb}$. It is evidence for an increasing X-ray burning area during the burst rise while the stellar surface cools off during the decay stage, see text.

X-ray light curve. This allows us to determine the correlation and estimate any time lag between X-ray and optical variability. The measurement of the cross-correlation function provides a characteristic delay which does not depend on particular model fitting. The results show that the optical burst lags the X-ray burst by ~ 4 s, which is marginally larger than expected in this system. The separation of the compact object and companion star is 2–3 light-s if we assume an orbital period of ~ 2.1 hr (Homer et al. 1998), a neutron star mass of $1.4 M_{\odot}$ and a companion star mass of 0.1 – $1.1 M_{\odot}$. However, in using a cross-correlation method we are essentially limited to the 5 s time resolution of the optical data (the PCA data have a much higher time resolution). Moreover, the delay appears to vary, from almost nothing at the start of the burst to a few seconds at the peak. This suggests that the delay might be a function of flux. Therefore a cross correlation analysis cannot provide a full picture of the delay between the X-ray and optical fluxes and instead we model the optical burst by convolving the X-ray light curve with a transfer function.

3.2.1.2 Transfer function

In order to model the time delay between the optical and X-ray bursts, we convolve a Gaussian transfer function with the X-ray light curve and use χ^2 fitting to model the optical light curve. The same method was used by Hynes et al. (1998) to model the *HST* light curve of GRO J1655–40 from the *RXTE* light curve. The Gaussian transfer function is given by:

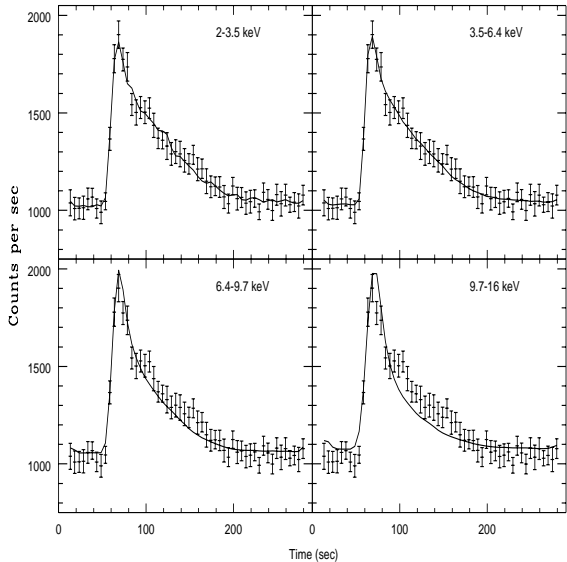
$$\psi(\tau) = \frac{\Psi}{\sqrt{2\pi\Delta\tau}} e^{-\frac{1}{2}(\frac{\tau-\tau_0}{\Delta\tau})^2} \quad (1)$$

where τ_0 is the mean time delay and $\Delta\tau$ is the dispersion or ‘smearing’ which is a measure of the width of the Gaussian. Ψ is the strength of the response.

We performed a series of convolutions of the transfer function with the lightcurves from the four energy bands, varying both τ_0 and $\Delta\tau$ independently. Essentially we adjust the overall delay and the degree of ‘smearing’, until

Table 5. Timing parameters of the simultaneous X-ray/optical burst by fitting linear-rise exponential-decay model.

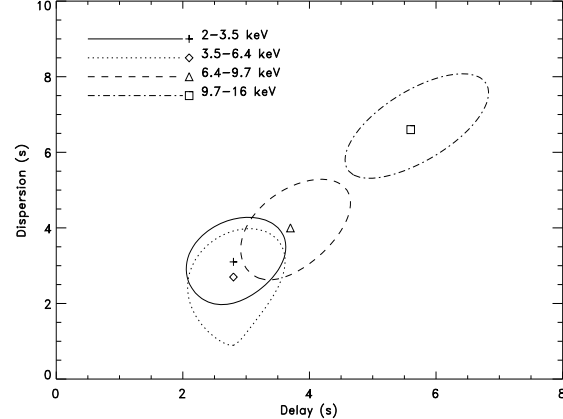
	2-3.5 keV	3.5-6.4 keV	6.4-9.7 keV	9.7-16 keV	Optical
Peak time (MJD)	50988.82510	50988.82511	50988.82512	50988.82512	50988.82516
Rise time (s)	7.2 ± 0.2	7.3 ± 0.2	7.81 ± 0.07	8.52 ± 0.05	10.7 ± 0.1
e-folding time (s)	59 ± 2	54.3 ± 0.9	35.6 ± 0.8	20.5 ± 0.7	55 ± 4

**Figure 8.** Best-fitting predicted light curves using a Gaussian transfer function on the four X-ray energy bands. The resulting curves are superimposed on the optical data points.

the transferred X-ray lightcurve reproduces the optical response. Finally, Figure 8 shows the best fit predicted light curves from each convolution superimposed on the optical light curve. The principal features of the optical burst profile are reproduced well in the predicted light curves from the 2-3.5 and 3.5-6.4 keV energy bands. Table 6 summarizes the results of the Gaussian transfer function fitting to all four energy bands. The fits are good ($\chi^2 < 1$ for 51 d.o.f.) for the two lower energy bands but not for the higher energy ones. The mean delay and dispersion between the optical and lower X-ray energy bands are both ~ 3 s (Table 6 and Figure 9). The strength of the response, Ψ , is almost the same for the two lower X-ray energy bands, at a value of ~ 0.0137 , while it is 2-3 times smaller for the higher X-ray energy band. This is an indication that a greater proportion of the reprocessing occurs at lower energies.

4 DISCUSSION

X-ray and optical bursts from GS 1826-24 were previously reported by Ubertini et al. (1999), In't Zand et al. (1999) and Homer et al. (1998). Our X-ray/optical observations of GS 1826-24 showed three X-ray bursts, of which two were observed by *ASCA*, whereas one was observed by *RXTE* simultaneously with the optical. On the basis of their spectral properties and time profiles, all the bursts have a cooling trend during their decays and exhibit blackbody spectra

**Figure 9.** Contour plot of the convolution with the *RXTE* light curves and Gaussian transfer function where the contour is defined as the 1σ confidence region.

with temperatures of a few keV. The time profiles show fast rise times of 7-9 s and long decay times ranging from 20-60 s depending on the energy band. We therefore interpret the three bursts detected from GS 1826-24 as type I bursts (Hoffmann et al. 1978). The relatively long rise time ($\sim 7-9$ s), as compared to bursts in other systems, indicates that the burst front may have enough time to spread over the whole neutron star surface during the rise to burst and suggests that the burning is homogeneous over the surface of the neutron star. This is consistent with the fact that we see no evidence for pulsations during the burst. We note that X-ray burst rise times in other sources have been observed to be smaller than ~ 6 sec (see e.g. Sztajno et al. 1986; Lewin et al. 1987), making this system rather unique. The burst rise times derived by In't Zand et al. (1999) range from 5-8 s which are also consistent with our observations.

For the simultaneous burst we may compare the ratio of the persistent to peak fluxes, in both the X-ray and optical, using the results of Lawrence et al. (1983). They derived a simple power law relation between the changes in U, B and V band fluxes and the corresponding X-ray flux variations during a well-studied burst of X1636-536, with $(\frac{F_{X,max}}{F_{X,pers}}) = (\frac{F_{opt,max}}{F_{opt,pers}})^\beta$, where β varies with passband. Our burst shows that $\beta \sim 4$ which is comparable to the value $\beta_V \sim 3$ found for X1636-536 in the V band, which is the closest approximation to our white light passband. Hence, we may imply that the reprocessed emission from the GS 1826-24 burst is also approximately that from a blackbody (with a temperature set by the degree of X-ray irradiation), where the optical passband is on the Rayleigh-Jeans tail (Lawrence et al. 1983).

The X-ray burst observed by RXTE shows evidence

Table 6. Summary of results from convolution of a Gaussian transfer function to the four different X-ray energy bands light curves

	2–3.5 keV	3.5–6.4 keV	6.4–9.7 keV	9.7–16 keV
τ_0 (s)	2.8 ± 0.7	2.8 ± 0.6	3.7 ± 0.7	5.6 ± 0.9
$\Delta\tau$ (s)	3.1 ± 1.3	$2.7^{+1.2}_{-1.7}$	4 ± 1	$6.1^{+1.2}_{-1.0}$
$\Psi(10^{-3})$	13.8 ± 6.2	$13.7^{+2.3}_{-4.1}$	7.0 ± 1.2	$4.5^{+0.7}_{-0.5}$
χ^2_ν (51 d.o.f.)	0.49	0.42	1.5	2.1

for an increase in the burning area during the early rise phase, but no evidence for photospheric radius expansion. Note that this is consistent with the fact that most X-ray bursts showing photospheric radius expansion have rise times less than ~ 1 sec (see Lewin et al. 1995). However, by assuming that our observed peak luminosity of $F_{max} = (2.8 \pm 0.4) \times 10^{-8}$ erg cm $^{-2}$ s $^{-1}$ is near the Eddington limit of $\sim 1.8 \times 10^{38}$ ergs s $^{-1}$ for a 1.4 M $_\odot$ neutron star, we can set an upper limit to the distance to GS 1826–24. We derive a maximum distance of $d = 7.5 \pm 0.5$ kpc. This estimate is consistent with the upper limit from *BepoSAX* NFI observations (7.4 ± 0.7 kpc; In't Zand et al. 1999) and the optical lower limit of 4 kpc (Barret et al. 1995). The luminosity ratios are $L_{pers}/L_{burst} \sim 55$ and ~ 50 for the bursts observed with *ASCA* and *RXTE*, respectively. This is comparable with that found by *BepoSAX* WFC (60 ± 7 ; Ubertini et al. 1999). Coupling this value with an estimated stable accretion rate of $\sim 1.5 \times 10^{-9}$ M $_\odot$ yr $^{-1}$ (Ubertini et al. 1999), the burst must involve a combined hydrogen-helium burning phase (Lewin, van Paradijs & Taam 1995). This relatively long burst also resembles the theoretical results of X-ray bursts driven by rapid proton capture process, or rp-process (see Hanawa & Fujimoto 1984; Taam 1981; Bildsten 1998; Schatz et al. 1998).

Pedersen et al. (1982) have shown that the optical burst mainly reflects the geometry of the system and that the contribution of intrinsic radiative processes is small. Hence the correlated optical and X-ray bursts discussed above are useful as probes of the structure and geometry of the compact object surroundings. Within the framework of the low-mass X-ray binary system, the reprocessing can occur in the accretion disk and the companion star. Based on our observed mean delay of 3 ± 1 s for the optical burst with respect to low energy X-rays, we can then constrain the orbital period of the system. By Kepler's law, the light travel time of 2–4 s corresponds to an orbital period of 1.6–5.5 hr if we assume a $1.4M_\odot$ neutron star and a companion star mass of 0.1 – $1.1M_\odot$ (i.e. for a low-mass main sequence star and stable mass transfer). Hence, this range of periods provides support for the 2.1 ± 0.1 hr orbital period proposed by Homer et al. (1998). Lastly, from only one simultaneous optical/X-ray burst, we cannot draw a firm conclusion as to whether the optical burst is due to reprocessing in the disk or on the surface of the companion star. However, given that the source is a low inclination system ($< 70^\circ$; Homer et al. 1998) and the ratio of smearing to delay is ~ 1 , the reprocessing is expected to be dominated by the accretion disk.

It is important in future studies to search for the possibly variable delays if the reprocessing occurs on the surface of the companion star (Matsuoka et al. 1984) or the 'thick spot' in the disk proposed by Pedersen et al. (1981). Whether the dominant reprocessor is the companion star

or the 'thick spot', one expects the ratio of optical to X-ray flux in a burst to vary periodically. Moreover, the optical delay would vary as a function of orbital phase as suggested by Pedersen, van Paradijs & Lewin (1981). Ubertini et al. (1999) recently proposed a 5.76-hr quasi-periodicity in the occurrence of X-ray bursts in GS 1826–24, which makes this problem difficult to resolve with current low-Earth-orbit satellites. However, with upcoming missions such as *Chandra* and *XMM*, much longer continuous X-ray coverage will be possible, and together with ground-based telescopes will enable us to probe the structure of this source in much greater detail.

ACKNOWLEDGEMENTS

We are grateful to Darragh O'Donoghue (SAAO) for his advice on the use of the UCT-CCD for high-speed photometry and his help with the subsequent reductions. We also thank Lars Bildsten for valuable comments and Fred Marang (SAAO) for his support at the telescope, and the *RXTE* SOC team for their efforts in scheduling the simultaneous time. This paper also utilizes results provided by the ASM/*RXTE* team.

REFERENCES

Barret, D., Motch, C., Pietch, W., 1995, *A&A*, 303 526
 Barret, D., McClintock, J.E., Grindlay, J.E., 1996, *ApJ*, 473, 963
 Bildsten, L., 1998, in *The Many Faces of Neutron Stars*, ed. A. Alpar, L. Buccieri, & J. van Paradijs, (Dordrecht: Kluwer)
 Bradt, H.V., Rothschild, R.E., Swank, J.H., 1993, *A&AS*, 97, 355
 Hanawa, T., Fujimoto, M.Y., 1984, *PASJ*, 36, 199
 Hoffman, J.A., Marshall, H., J.A., Lewin, W.H.G., 1978, *Nature*, 271, 630
 Homer, L., Charles, P.A., O'Donoghue, D., 1998, *MNRAS*, 298, 497
 Homer, L., et al., 1999, in preparation (paper II)
 Hynes, R.I., O'Brien, K., Horne, K., Chen, W., Haswell, C.A., 1998, *MNRAS*, 299, L37
 In't Zand, J.J.M., 1992, PhD thesis, University of Utrecht
 In't Zand, J.J.M., Heise, J., Kuulkers, E., Bazzano, A., Cocchi, M., Ubertini, P., 1999, *A&A*, 347, 891
 Lawrence, A., Cominsky, L., Engelke, C., et al., 1983, *ApJ*, 271, 793.
 Lewin, W.H.G., van Paradijs, J., Taam, R.E., 1995, in *X-ray Binaries*, ed. W. Lewin, J. van Paradijs & E. van den Heuvel (Cambridge: Cambridge Univ. Press), P.175
 Lewin, W.H.G., Penninx, W., Paradijs, J., et al., 1987, *ApJ*, 319, 893
 London, R., Taam, R.E., Howard, M., 1984, *ApJ*, 287, L27
 Makino, F., et al., 1988, *IAUC* 4653
 Matsuoka, M., Mitsuda, K., Ohashi, T. et al., 1984, *ApJ*, 283, 774
 Motch, C., et al., 1994, *IAUC* 6101

O'Donoghue, D., 1995, Baltic Astronomy, 4, 519

Pedersen, H., van Paradijs, J., Lewin, W.H.G., 1981, Nature, 294, 725

Pedersen, H., Lub, J., Inoue, H., et al., 1982, ApJ, 263, 325

Schatz, H., Aprahamian, A., Görres, J., et al., 1998, Physics Reports, 294, 167

Stetson, P.B., 1987, Pub. Astron. Soc. Pac., 99, 191

Strickman, M., et al., 1996, A&AS, 120, 217

Strohmayer, T.E., Zhang, W., Swank, J.E., 1997, ApJ, 487, L77

Sztajno, M., van Paradijs, J., Lewin, W.H.G., Trümper, J., Stollman, G., Pietsch, W., van der Klis, M., 1985, ApJ, 299, 487

Sztajno, M., van Paradijs, J., Lewin, W.H.G., Langmeier, J., Trümper, J., Pietsch, W., 1986, MNRAS, 222, 499

Taam, R.E., 1981, ApJ, 247, 257

Tanaka, Y., 1989, in Two topics in X-ray astronomy, 23rd ESLAB Symposium., P.3, ESA: Paris, Bologna

Tanaka, Y., Inoue, H., Holt, S.S., 1994, PASJ, 46, L37

Tanaka, Y., Lewin, W.G.A., 1995, in X-ray Binaries, Cambridge University Press, eds. Lewin W.H.G., van Paradijs, J. & van den Heuvel, E.P.J., P.126

Ubertini, P., et al., 1999, ApJ, 514, L27

van Paradijs, J., Lewin, W.H.G., 1985, A&A, 157, L10

van Paradijs, J., Sztajno, M., Lewin, W.H.G., Trümper, J., Vacca, W.D., van der Klis, M., 1986, MNRAS, 221, 617